Photoactivity and Stability of $WO_3/BiVO_4$ Photoanodes: Effects of the Contact Electrolyte and of Ni/Fe Oxyhydroxide Protection

*Ivan Grigioni, Annamaria Corti, Maria Vittoria Dozzi and Elena Selli**

Dipartimento di Chimica, Università degli Studi di Milano, via Golgi 19, I-20133 Milano, Italy

ABSTRACT: Photoelectrodes with the $WO_3/BiVO_4$ heterojunction architecture are among the most efficient semiconductor oxide-based photoanodes for water oxidation. However, because of the different experimental conditions employed in their photoelectrochemical characterization (in particular the nature and concentration of the contact electrolyte and the pH of the solution), a direct and unambiguous comparison of their performance obtained in different labs is often quite difficult. In this work, we systematically tested identical $WO_3/BiVO_4$ photoanodes in contact with solutions of the most commonly used electrolytes, *i.e.* Na_2SO_4 and the potassium phosphate buffer (KPi), at various electrolyte concentration and pH. Furthermore, $WO_3/BiVO_4$ photoanodes protected with a Ni/Fe oxyhydroxide oxygen evolution catalyst were also tested under identical conditions. In contact with KPi solutions, both unprotected and protected electrodes produce higher photocurrent than in contact with Na_2SO_4 solutions, but they proved to be less stable, particularly under basic conditions. $WO_3/BiVO_4$ heterojunction systems modified by deposition of the Ni/Fe oxyhydroxide co-catayst proved to be more stable and to produce higher photocurrent, with a cathodic shift of the photocurrent onset.

INTRODUCTION

$BiVO_4$ is an excellent visible light absorbing material suitable to fabricate photoanodes for solar light induced water splitting. From the first application of this material to water oxidation,[1,2] the photoconversion efficiency of $BiVO_4$ rapidly increased through the development of effective charge extraction strategies, mainly based on the formation of heterojunction films in which $BiVO_4$ is combined with an electron acceptor layer (*i.e.* WO_3, ZnO, TiO_2 and $CuWO_4$)[3–6] or on the improvement of the poor electron transport properties of $BiVO_4$ by doping.[7–9] Furthermore, the deposition of co-catalysts for the oxygen evolution reaction (OER) boosts the photoelectrochemical properties of the underlayer by mediating the hole extraction across the photoexcited semiconductor–electrolyte interface.[10] This in turn enhances the photoconversion efficiency and prevents the photoxidation of the photoanode, ensuring prolonged stability.

After the use of iridium oxides[11,12] and cobalt-based oxides,[13,14] oxyhydroxides of earth abundant elements such as nickel and iron are now recognized as the most effective OER catalysts employed so far.[15–18] Photoelectrodeposited FeOOH increase the rate of water oxidation on $BiVO_4$ with considerable photocurrent density improvement and substantial stability.[19] The combination of FeOOH with NiOOH in multilayered structures enhances the efficiency of undoped $BiVO_4$ films providing stable photocurrent under simulated solar light conditions.[16] Mixed transition (oxy)hydroxides catalysts proved to be thermodynamically more stable under OER conditions than the corresponding oxides and Fe impurities within Ni or Co scaffolds highly enhance the catalyst activity.[15,20] Moreover, new deposition techniques employing soft conditions were developed, leading to complete covering of the underlying oxide.[17,21] Among these strategies photoelectrochemical approaches offer the advantage of photoactive sites preferential coverage.[19,22]

In general, $BiVO_4$- and $WO_3/BiVO_4$-based photoanodes can be synthesized by different ways and are mostly tested under standardized irradiation conditions (1 sun) through an AM 1.5 G filter, but different experimental conditions, *i.e.* the electrolyte in contact with the photoanode and also its concentration, are employed.[3,4,9,14,23–32] This hampers a direct comparison of the performances reported for the same coupled material by different research groups. Na_2SO_4 and the phosphate (KPi) buffer are by far the most largely employed electrolytes, although other electrolyte solutions (for example the recently employed carbonate or borate buffers when cobalt carbonate or cobalt borate are employed as co-catalysts) were found to enhance the activity of oxygen evolution catalysts.[33–36] Thus, the question arises: how does the same $WO_3/BiVO_4$ electrode perform in contact with different electrolyte solutions?

To answer this question, in this work we systematically investigate the photoelectrochemical properties of identical unprotected $WO_3/BiVO_4$ heterojunction electrodes in contact with Na_2SO_4 or KPi solutions and compare the photocurrent density recorded during linear sweep voltammetry scans and chronoamperometry experiments (at 1.23 V *vs.* RHE) on a heterojunction electrode immersed in each electrolyte under simulated solar light irradiation.[37] This systematic screening is extended to $WO_3/BiVO_4$ photoanodes coated with a nickel/iron-based oxygen evolution catalyst and the results are compared with those obtained with the unprotected $WO_3/BiVO_4$ heterojunction system, to highlight the effects of the NiFe based co-catalyst on its efficiency and stability.

EXPERIMENTAL SECTION

Materials. The following chemicals were employed: tungsten(VI) ethoxide 99.8% (5% w/v in ethanol), ammonium vanadium oxide, bismuth(III) nitrate pentahydrate ACS 98%, benzyl alcohol ACS 99% (Alpha Aesar), ethyl cellulose (MP Biomedics), poly(vinyl alcohol) >99%,

citric acid 99%, $FeSO_4$ 98% (Aldrich), glacial acetic acid, anhydrous sodium sulfate and sodium sulphite (Fisher Scientific).

Photoelectrodes preparation. The $WO_3/BiVO_4$ photoanodes were prepared as already described,[38] by first depositing a WO_3 layer on a fluorine-doped tin oxide (FTO) glass electrode, followed by $BiVO_4$ deposition. Briefly, 1.0 mL of tungsten ethoxide, 5 wt% in ethanol, was added to 42 mg of citric acid acting as stabilizer inside a glovebox to avoid tungsten ethoxide hydrolysis. Once citric acid was completely dissolved, benzyl alcohol (0.3 mL) and ethyl cellulose (40 mg) were added to the solution, which was stirred for one hour at 70 °C and then overnight at room temperature to attain the complete swelling of ethyl cellulose. The so obtained paste (with a 0.085 M tungsten content) is stable for several weeks. 100 μL of the paste were deposited on a 2.5 x 2.5 cm^2 FTO glass electrode, by spin coating at 6000 rpm for 30 s. The final spinning rate was reached with a three acceleration step program, *i.e.* 500 rpm s^{-1} up to 1000 rpm, then 1000 rpm s^{-1} up to 3000 rpm and finally 3000 rpm s^{-1} up to 6000 rpm. Prior to deposition, the FTO glass was cleaned by 15 min-long sonication, first in a soap aqueous solution, then in ethanol and finally in water. After coating, the so obtained film was dried at 80 °C for 1 h and then annealed at 500 °C for 1 h.

The $WO_3/BiVO_4$ combined photoanodes were prepared by coating the so obtained WO_3 electrodes with a $BiVO_4$ film, according to a procedure similar to that reported elsewhere.[39] Typically, 0.002 mol of $Bi(NO_3)_3$ and NH_4VO_3 were added to 6 mL of 23.3% HNO_3 containing 0.004 mol of citric acid. A denser paste was obtained by adding 0.04 g of poly(vinyl alcohol) and 0.25 mL of acetic acid to 1.0 mL of the above solution, and the mixture was stirred to allow complete poly(vinyl alcohol) dissolution. A $BiVO_4$ layer was obtained by spin coating the paste at 4000 rpm for 30 s on FTO/WO_3. The so-obtained film was then dried for 1 h at 80 °C and

annealed for 1 h at 500 °C. In order to limit any day to day variation in the deposition procedure, all $WO_3/BiVO_4$ photoanodes used in our investigation were prepared on the same day.

Deposition and activation of the Ni-Fe oxyhydroxy oxygen evolution catalyst. In order to protect the $WO_3/BiVO_4$ photoanodes and enhance their photoelectrochemical performance a mixed nickel and iron oxyhydroxides co-catalyst layer was deposited on their surface. NiOOH and FeOOH were sequentially deposited through the technique reported by Shi *et al.*[22]

FeOOH was first deposited from an aqueous 0.1 M $FeSO_4$ solution via a photoelectrochemical assisted deposition, under 1 sun AM 1.5 G irradiation, at a constant potential of 0.25 V *vs.* Ag/AgCl for 13 min. A fresh iron sulfate solution was employed in each deposition to avoid the formation of Fe oxide and hydroxide colloids. A first NiOOH layer was obtained by polarizing the $WO_3/BiVO_4$/FeOOH electrode at 0.11 V *vs.* Ag/AgCl for 6 min in contact with a $NiSO_4$ 0.1 M solution; its pH was adjusted to 6.7 with NaOH (*ca.* 70 μL of NaOH 0.1 M were added to a 50 mL $NiSO_4$ solution). Finally an additional NiOOH layer was deposited from the same solution at 1.2 V *vs.* Ag/AgCl for 90 s without irradiation.

After deposition the Ni-Fe oxyhydroxide (NiFe) co-catalyst was activated in order to attain a stable photocurrent from the heterojunction. Indeed, by performing consecutive linear sweep voltammetry runs with the $WO_3/BiVO_4$/NiFe electrode its overall performance was found to increase (see Figure SI1). Therefore, prior to any photoelectrochemical test in different electrolyte solutions, the $WO_3/BiVO_4$/NiFe photoanodes were activated by performing a 120 min-long chronoamperometry in the 0.5 M Na_2SO_4 and/or KPi solutions. Two examples of this activation treatment are reported in Figure SI2.

Optical, structural and photoelectrochemical tests. UV−visible absorption spectra were recorded using a Jasco V-670 spectrophotometer. The crystalline phase of the materials was

determined through X-ray powder diffraction (XRPD) analysis using a Philips PW1820 with Cu Kα radiation at 40 mA and 40 kV. Field-emission scanning electron microscopy (FESEM) images were collected by using a Zeiss SUPRA 40 scanning electron microscope, operating at a 5−7 kV accelerating voltage, at a 3−4 mm working distance. A series of low and high magnification images were collected before and after irradiation. Elemental analyses were performed by using an energy dispersive X-ray detector (Oxford instruments) operating at a 10 kV voltage and a working distance of 9 mm.

Photoelectrochemical measurements were carried out using a three electrode cell with an Ag/AgCl (3.0 M NaCl) reference electrode, a platinum gauze as a counter electrode, and a Princeton Applied Research 2263 (PARstat) potentiostat. The photoanodes were tested under back side illumination (through the FTO/WO_3/$BiVO_4$ interfaces). The light source was an Oriel, Model 81172 solar simulator providing AM 1.5 G simulated solar illumination with 100 mW cm^{-2} intensity (1 sun). The irradiated area of the electrode was 0.28 cm^{-2}. The potential *vs.* Ag/AgCl was converted into the RHE scale using the Nernst equation:

$$E_{RHE} = E_{AgCl} + 0.059\ pH + E^{o}_{AgCl}, \text{ with } E^{o}_{AgCl} \text{ (3.0 M NaCl)} = 0.210\ V \text{ at } 25\ ^{\circ}C \qquad (1)$$

A 250 W medium pressure iron halogenide mercury arc lamp (Jelosil HG 200, emission spectrum shown in Figure SI3) was employed in some experiments to test the effect of higher intensity irradiation with a larger UV component.

The photoactivity and the stability of each electrode were evaluated by recording in each electrolyte both a linear sweep voltammetry curve with a 10 mV s^{-1} scan rate and a 22 min-long chronoamperometry trace at 1.23 V *vs.* RHE at pH 7. Different concentrations of each electrolyte were tested, in the 0.005-0.5 M range. At the optimal 0.05 M KPi buffer concentration additional photoelectrochemical tests were made at pH 6 and pH 8 by modulating the K_2HPO_4 *vs.* KH_2PO_4

concentration ratio in the phosphate buffer. For the unprotected heterojunction films a fresh electrode was used when testing the effect of each electrolyte solution. Conversely, when screening the performance of WO_3/$BiVO_4$/NiFe photoanodes, only two electrodes, one for the Na_2SO_4 and one for the KPi electrolyte, were employed in the photoelectrochemical measurements at pH 7, starting from the more concentrated solution (0.5 M) up to the more diluted one (0.005 M), which were obtained through successive dilution without changing the photoanode, nor its position, followed by homogenization of the electrolyte solution. Before performing these tests with the NiFe-protected photoanodes, the OER co-catalyst, after its deposition on the naked WO_3/$BiVO_4$ photoanode, was activated at the highest electrolyte concentration by consecutive linear sweep voltammetry scans until a stable photocurrent was reached, followed by a 120 min-long chronoamperometry scan (1.23 V *vs.* RHE). After this activation procedure, the final linear sweep voltammetry curve was recorded, followed by a 22-min-long chronoamperometry. Then, after dilution to the next desired concentration, the linear sweep voltammetry curve and the 22 min-long chronoamperometry trace were recorded in contact with a lower concentration solution.

RESULTS AND DISCUSSION

Morphological characterization of the electrodes. The top views in SEM analysis of the WO_3/$BiVO_4$ film and their magnification reported in Figures 1A and 1A' show an aggregated network of particles, with morphological features similar to those obtained for $BiVO_4$ films prepared by the same procedure.[27,38] The successful deposition of a mixed nickel and iron oxyhydroxide co-catalyst layer is confirmed by the appearance of peculiar bright nanometric agglomerates homogeneously distributed on the photoanode surface (see Figures 1B and 1B'), similar to those previously reported by others.[25] Energy dispersive X-ray (EDX) analysis did not

evidence any signal associated to the presence of Fe and Ni on the surface, very reasonably because their amount is below the instrumental detection limit. Furthermore, by comparing the images shown in Figures 1C and 1C' with those shown in Figures 1B and 1B', one can verify that no significant variation of the original morphology of the surface occurred during the photoelectrochemical characterization tests of the NiFe protected $WO_3/BiVO_4$ photoanodes.

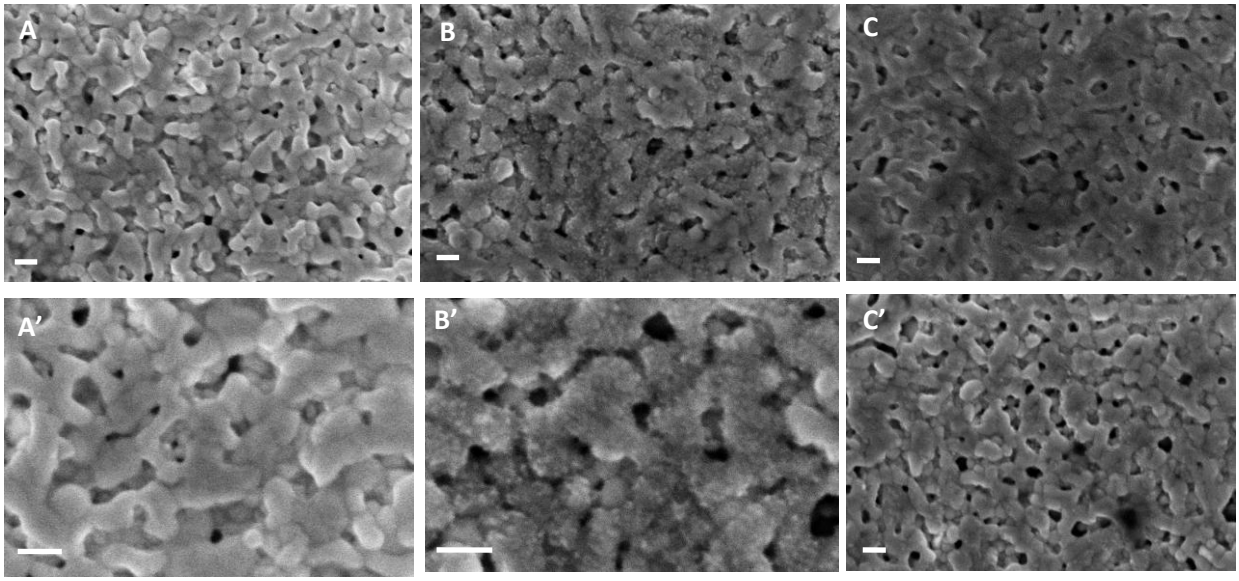

Figure 1. Top view FESEM images of the $WO_3/BiVO_4$ photoanode (A, A') as prepared and (B, B') after its protection with a mixed nickel and iron oxyhydroxide co-catalyst layer. Images C and C' refer to the $WO_3/BiVO_4$/NiFe photoanode after its photoelectrochemical characterization in contact with a 0.5 M Na_2SO_4 solution at pH 7. A', B' and C' are higher magnification images of the same photoanode shown in images A, B and C, respectively, the scale bar is 100 nm.

Photoelectrochemical performance of $WO_3/BiVO_4$ electrodes. The preparation of the $WO_3/BiVO_4$ photoanode series gave well reproducible results as testified by the similar UV-Vis absorption spectra of films prepared in the same day (see Figure SI4).

Na_2SO_4 is the aqueous electrolyte by far mostly employed in photoelectrochemical measurements at neutral pH.[27,39–43] Figures 2A and 2B show the current density measured with

$WO_3/BiVO_4$ electrodes immersed in 0.005-0.5 M Na_2SO_4 solutions at pH 7. The electrolyte concentration has negligible effect on the photocurrent potential onset, while it strongly affects the current density. In fact, in the two most diluted 0.005 and 0.01 M electrolyte solutions, the $WO_3/BiVO_4$ photoanode produces low photocurrents, almost linearly increasing with increasing

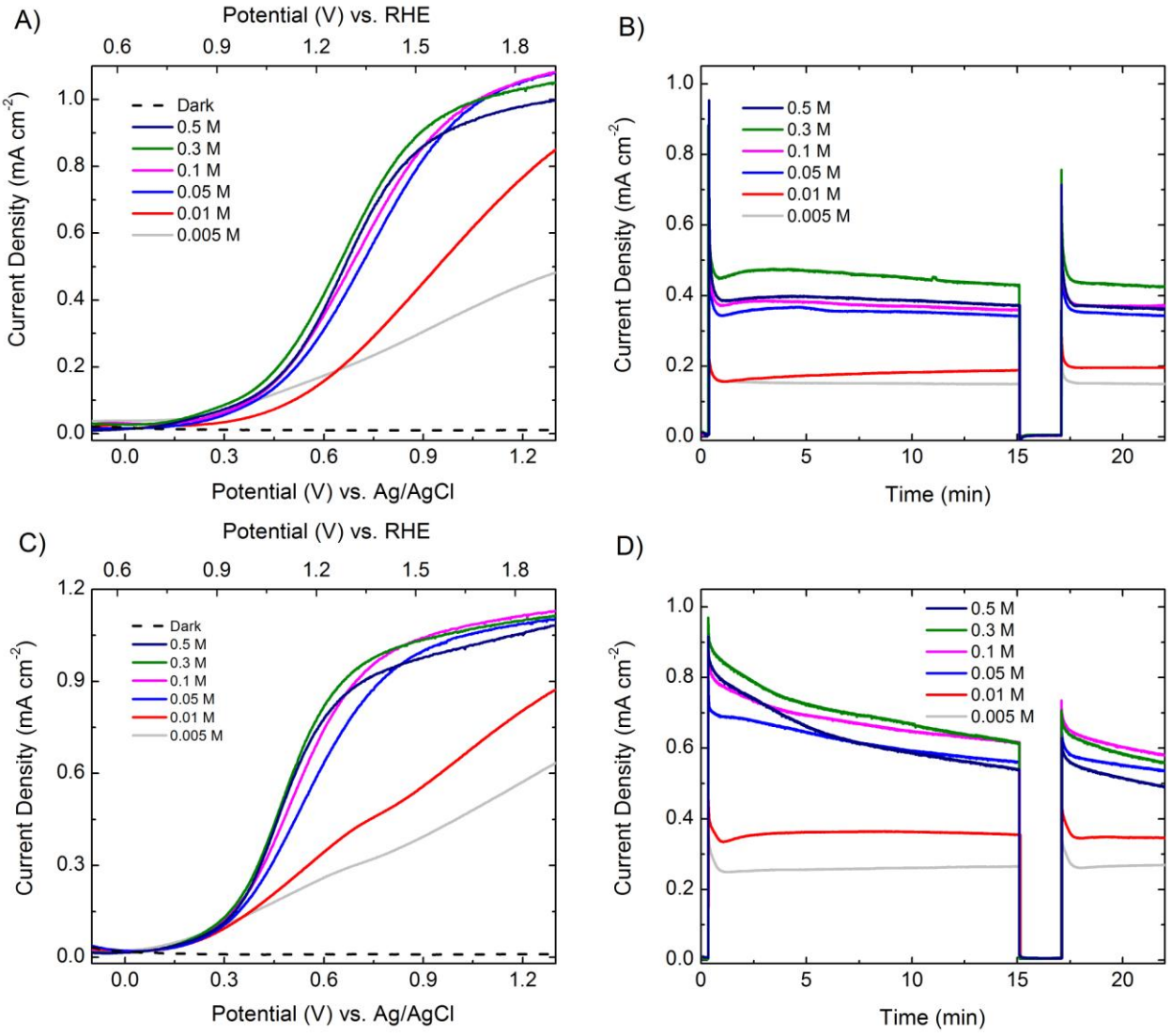

Figure 2. Photoelectrochemical characterization under AM 1.5 G simulated solar light irradiation of the $WO_3/BiVO_4$ electrodes in contact with (A, B) Na_2SO_4 and (C, D) KPi solutions at pH 7. (A ,C) Linear sweep voltammetry and (B, D) chronoamperometric measurements recorded at 1.23 V *vs.* RHE.

applied bias, as a consequence of the high ohmic drop due to the resistivity of the electrolyte, which is inversely proportional to the electrolyte concentration. Higher photocurrent values are measured when the photoanode is in contact with electrolyte concentrations above 0.05 M and the applied bias more strongly affects the photoelectrochemical response. At these electrolyte concentrations a saturation photocurrent is attained at potentials above *ca.* 0.9 V *vs.* Ag/AgCl, suggesting that at higher potentials the photocurrent is mostly limited by the surface oxygen evolution reaction rather than by internal charge carrier transport and recombination issues. The photocurrent density increases with the electrolyte concentration and has a maximum for the 0.3 M Na_2SO_4 solution, while lower values are obtained in contact with the 0.5 M Na_2SO_4 electrolyte solution.

The photoanode stability was evaluated in chronoamperometry experiments at a potential of 1.23 V *vs.* RHE (corresponding to 0.61 V *vs.* Ag/AgCl for pH 7 solutions), *i.e.* at the formal potential for water oxidation to O_2.[37] As shown in Figure 2B, the measured photocurrent density values parallel those recorded in linear sweep scan experiments (Figure 2A), the highest values being obtained with $WO_3/BiVO_4$ in contact with the 0.3 M Na_2SO_4 electrolyte. For Na_2SO_4 concentrations higher than 0.01 M, after the initial current drop in the first tenths of second following the beginning of irradiation, the photocurrent remains substantially stable during the test, with only a 5% photocurrent decrease with respect to the maximum value attained after the initial spike.

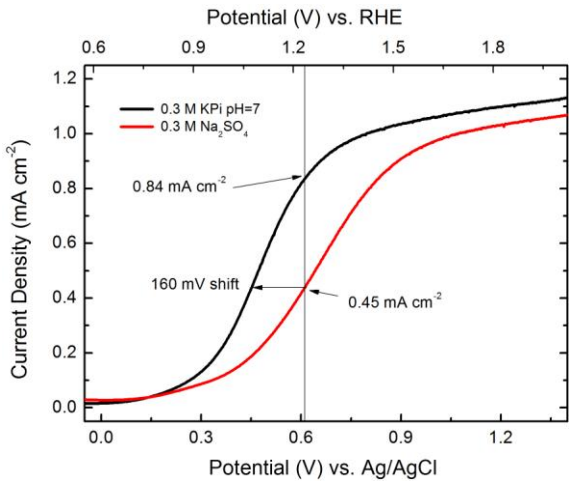

Figure 3. Comparison between the linear sweep voltammetry curves recorded with $WO_3/BiVO_4$ photoanodes in contact with the optimal 0.3 M KPi and Na_2SO_4 electrolyte concentration (red and black lines, respectively. The vertical line denotes 1.23 V *vs.* RHE, the formal potential of water oxidation.

The linear sweep voltammetry curves recorded with the photoanode in contact with different concentrations of phosphate buffer (KPi) at pH 7 are shown in Figure 2C. Also in this case the photocurrent grows with increasing electrolyte concentration and the highest photocurrent is obtained in contact with the 0.3 M KPi solution. By comparing the linear sweep voltammetry scans recorded with the $WO_3/BiVO_4$ electrode in contact with 0.3 M solutions of the Na_2SO_4 and KPi electrolytes (see Figure 3), the $WO_3/BiVO_4$ coupled system appears to perform better when it is in contact with the KPi solution, with a 160 mV cathodic shift of the photocurrent onset and an almost double current value at 1.23 V *vs.* RHE. However, the chronoamperometry experiments reported in Figure 2D suggest that this superior performance may be due to a KPi electrolyte-mediated photoanode self-oxidation. Indeed, the photocurrent obtained with the heterojunction electrode exhibits a faster decrease, the higher is the KPi concentration in the contact solution, dropping to 45%, 37%, 35% and 33% of its initial value with the photoanode in contact with 0.5, 0.3, 0.1 and 0.05 M KPi solutions. Moreover, although the current values

recorded in contact with the KPi are higher than those attained in contact with Na_2SO_4 solutions, chronoamperometry experiments indicate that in KPi the photocurrent stability is lower than in Na_2SO_4 solutions (compare Figures 2B and 2D). Indeed, very recent studies demonstrate that bismuth vanadate suffers from chemical and photochemical instability in contact with the KPi buffer[44] and that a bismuth phosphate layer forms on the $BiVO_4$ surface under illumination.[45]

Furthermore, the anodic current spikes in the traces shown in Figure 2D are smaller than those observed in contact with Na_2SO_4 solutions (Figure 2B). These photocurrent transient signals, appearing in the first tenths of second after the beginning of irradiation, are ascribed to surface holes accumulation due to the slow water oxidation kinetics.[46] In fact, immediately after photoexcitation, conduction band electrons are massively transferred to the external circuit producing high photocurrent values. On the other hand, photogenerated holes do not efficiently react with water molecules and accumulate at the electrode/electrolyte interface. This enhances photogenerated charge carriers recombination and leads to the high photocurrent spikes observed in Figure 2B, followed by a fast photocurrent decrease. Therefore, the smaller initial photocurrent spikes observed when photocurrent is recorded in contact with KPi solutions indicate a reduced accumulation of surface holes when the photoanode is in contact with KPi solutions. This evidence, combined with the lower photostability observed in chronoamperometry experiments performed in KPi, supports the hypothesis that in contact with this electrolyte the holes photogenerated in the film are consumed in a self-oxidation process, with the $WO_3/BiVO_4$ layer acting as a self electron donor. On the short term, *i.e.* in linear sweep voltammetry measurements, this leads to higher photocurrent values with respect to those recorded in contact with Na_2SO_4 solutions (compare Figure 2A and 2C), while on the long term

(see chronoamperometric measurements) a photocurrent decrease is observed as the photoanode material gets progressively oxidized.

The hypothesis of a progressive corrosion of the $WO_3/BiVO_4$ photoanodes in contact with KPi solutions is supported by EDX analysis, clearly showing a significant decrease of both Bi and W signals in the material after photoelectrochemical test experiments (see Figure SI5A and SI5B). On the contrary, the elemental composition of $WO_3/BiVO_4$ photoanodes remains substantially unchanged after their photoelectrochemical characterization in contact with Na_2SO_4 electrolyte solutions at pH 7 (see Figures SI5C and SI5D).

The pH value of the KPi buffer solution can be easily tuned in the 6-8 range and KPi solutions at different pH are often employed in photoelectrochemical tests.[13,14,47] Therefore the photoelectrochemical performace of our $WO_3/BiVO_4$ photoanodes was also tested in 0.05 M KPi solutions at pH 6 and 8. Such KPi concentration was chosen because it is the lowest KPi concentration ensuring photocurrent densities unaffected by the ohmic resistance drop of the solution, while higher KPi concentrations have negative effects on the photoanode stability (see Figure 2D). The linear sweep voltammetry curves (against Ag/AgCl) reported in Figure 4A show an anodic shift of the photocurrent onset with decreasing the pH value.[48,49] On the other hand, the photocurrent curves measured at different pH are almost superimposed (see inset in Figure 4A), if the applied potential is referred to RHE through the Nernst equation (eq. 1). Furthermore, while a neutral or slightly acidic pH does not affect markedly the photoanode stability in KPi solution (Figure 4B), the lowest photocurrent value is recorded at the end of the chronoamperometric test with the electrode in contact with the KPi solution at pH 8.

To get a deeper insight into stability *vs.* pH issues, chronoamperometry experiments were performed with freshly made electrodes employing a higher intensity UV irradiation source (see

Figure SI3). The number of more energetic photons absorbed per unit time by the $WO_3/BiVO_4$ photoanode under such irradiation conditions is more than doubled with respect to the number of lower energy photons absorbed under the AM 1.5 G simulated solar irradiation employed in all other experiments. Under such conditions the photostability of the photoanodes in contact with

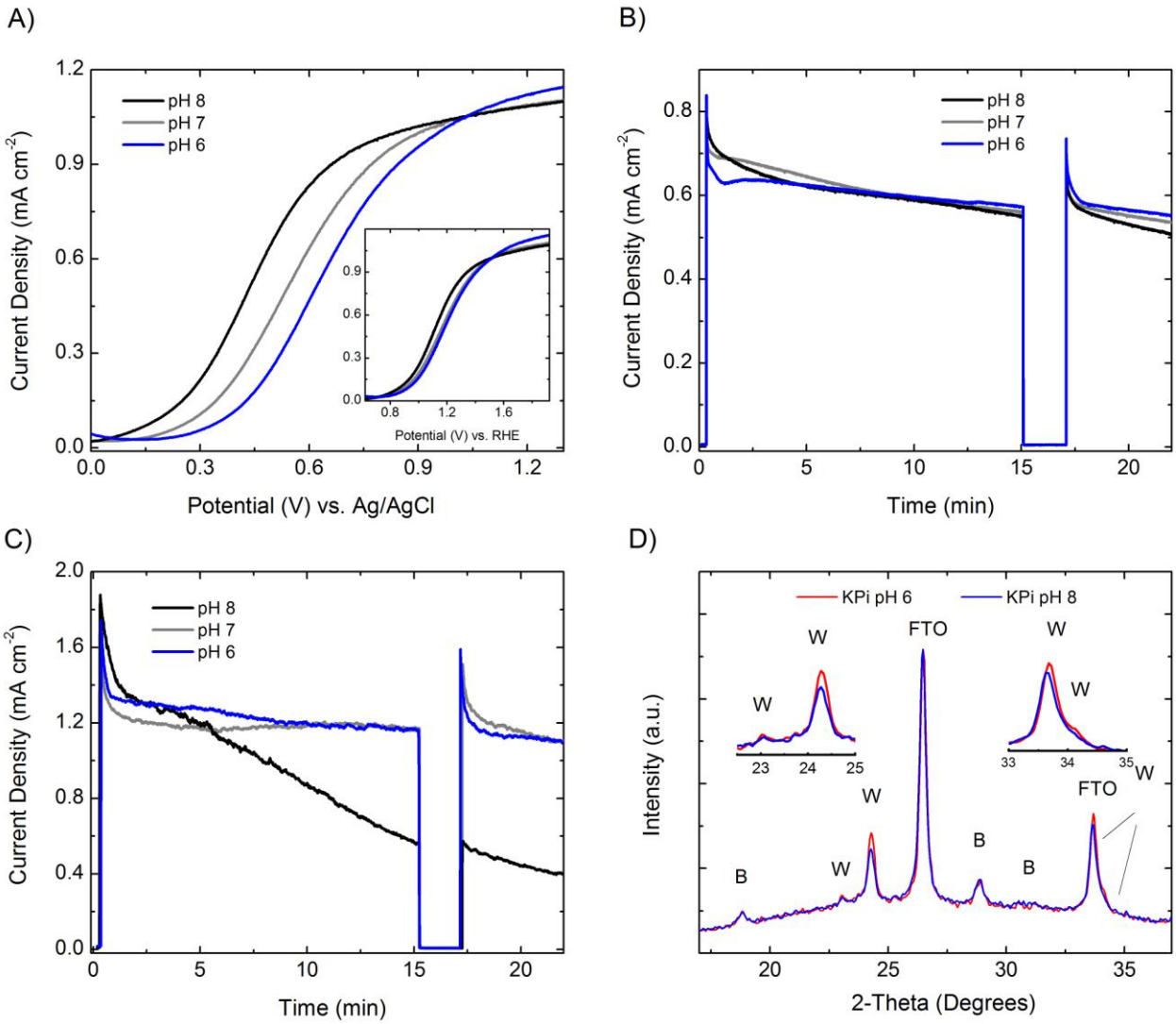

Figure 4. (A) Linear sweep voltammetry and (B) chronoamperometry curves recorded at 1.23 V *vs.* RHE with the $WO_3/BiVO_4$ electrode in KPi solutions at pH 6, 7 and 8 under AM 1.5 G irradiation and (C) high intensity UV irradiation. (D) XRPD analysis of the $WO_3/BiVO_4$ electrodes after stability tests in KPi solutions at pH 6 and 8; the diffraction patterns due to WO_3 and $BiVO_4$ are labeled as W and B, respectively; the two insets show magnifications of the 2-theta areas in which monoclinic WO_3 presents its more intense reflections.

the KPi solutions at pH 6 and 7 remains almost unaltered (see Figure 4C in comparison with Figure 4B), while a dramatic drop of the photocurrent recorded in contact with the KPi solution at pH 8 is observed, the photocurrent measured at the end of the test being only 20% of its initial value (Figure 4C). A possible explanation of this effect can be found in the well known instability of WO_3 in basic environment,[50] a hypothesis which finds confirmation through the XRPD analyses of $WO_3/BiVO_4$ electrodes after their stability tests in KPi solutions under high intensity UV light irradiation. Indeed, as shown in Figure 4D, a comparison between the XRPD spectra recorded with the two photoanodes tested under such irradiation conditions in contact with KPi solutions at pH 6 and 8 indicates that the diffraction patterns of WO_3 are less intense in the XRPD spectrum of the film tested in contact with the KPi solution at pH 8, confirming that the WO_3 underlayer undergoes photoinduced dissolution at this pH value.

Photoelectrochemical performance of the protected $WO_3/BiVO_4$/NiFe electrodes. We then extended our systematic study to $WO_3/BiVO_4$ heterojunction electrodes protected with amorphous Ni and Fe-based oxyhydroxyde (NiFe) oxygen evolution co-catalysts, which are among the most promising candidates as multimetal catalysts for the OER, allowing also to decrease the overpotential necessary to drive water oxidation.[20] Nickel, iron and Ni/Fe oxyhydroxides can be easily coated onto photoanodes through several soft deposition techniques such as low pressure methods,[21,51] electrochemical,[15] hydrothermal,[17] and photoelectrochemical approaches.[16,19] Here we deposited the NiFe OER catalyst onto fresh, unused $WO_3/BiVO_4$ heterojunction films by a well established photoelectrochemical method which ensures prolonged stability of $BiVO_4$ and $WO_3/BiVO_4$ electrodes.[22,25]

We found that the NiFe modified $WO_3/BiVO_4$/NiFe heterojunction photoanodes need to be activated with Na_2SO_4 solutions in order to generate an optimal and stable photocurrent. We thus

performed a 2 h-long irradiation of the protected electrodes in the two most concentrated (0.5 M) electrolyte solutions before performing the photoelectrochemical tests in contact with more diluted solutions. During activation the photocurrent generated by the photoanodes remains substantially unchanged when they are in contact with the Na_2SO_4 solution, whereas it moderately decreases in contact with the KPi solution (see Figure SI2). This implies that, with respect to pristine electrodes, the NiFe co-catalyst efficiently protects the photoanode toward self-oxidation (see also Figure SI6, reporting the results of a 4 h-long stability test in 0.5 M Na_2SO_4). Furthermore, with the protected photoanodes, especially if in contact with the Na_2SO_4 electrolyte, transient photocurrent spikes are smaller than those observed with the unprotected electrodes, suggesting a reduced accumulation of holes in the presence of the oxygen evolution catalyst. As already mentioned, no significant variation to the original morphology of the $WO_3/BiVO_4$ heterojunction electrode occurs under such conditions (Figure 1).

The activated $WO_3/BiVO_4$/NiFe films were then tested in contact with the two electrolytes, starting from the highest (0.5 M) down to the lowest (0.005 M) electrolyte concentration. As in the case of the unprotected photoanodes, the photoactivity measured in contact with the two most diluted Na_2SO_4 solutions is limited by the ohmic drop and the photocurrent linearly increases with increasing applied bias (Figure 5A). On the other hand, the photocurrent measured in the 0.05 and 0.1 M solutions reaches a saturation value around 0.8 V *vs.* Ag/AgCl. However, a progressive increase in electrolyte concentration leads to a strong enhancement of the photocurrent density and to an onset potential which is cathodically shifted by several mV. Moreover, unlike unprotected photoanodes, the $WO_3/BiVO_4$/NiFe electrode in contact with the 0.5 M Na_2SO_4 solution performs remarkably better than in contact with the 0.3 M Na_2SO_4 solution. This improvement in performance, as well as those obtained by increasing the Na_2SO_4

concentration from 0.1 to 0.3 M, should not be related only to the electrolyte conductivity increase, but mainly to an increased water oxidation rate on the NiFe surface. The results of the stability tests performed at 1.23 V *vs.* RHE (*i.e.*. at 0.61 V *vs.* Ag/AgCl) reported in Figure 5B match the trend found in linear sweep voltammetry scans. The photocurrents measured in contact

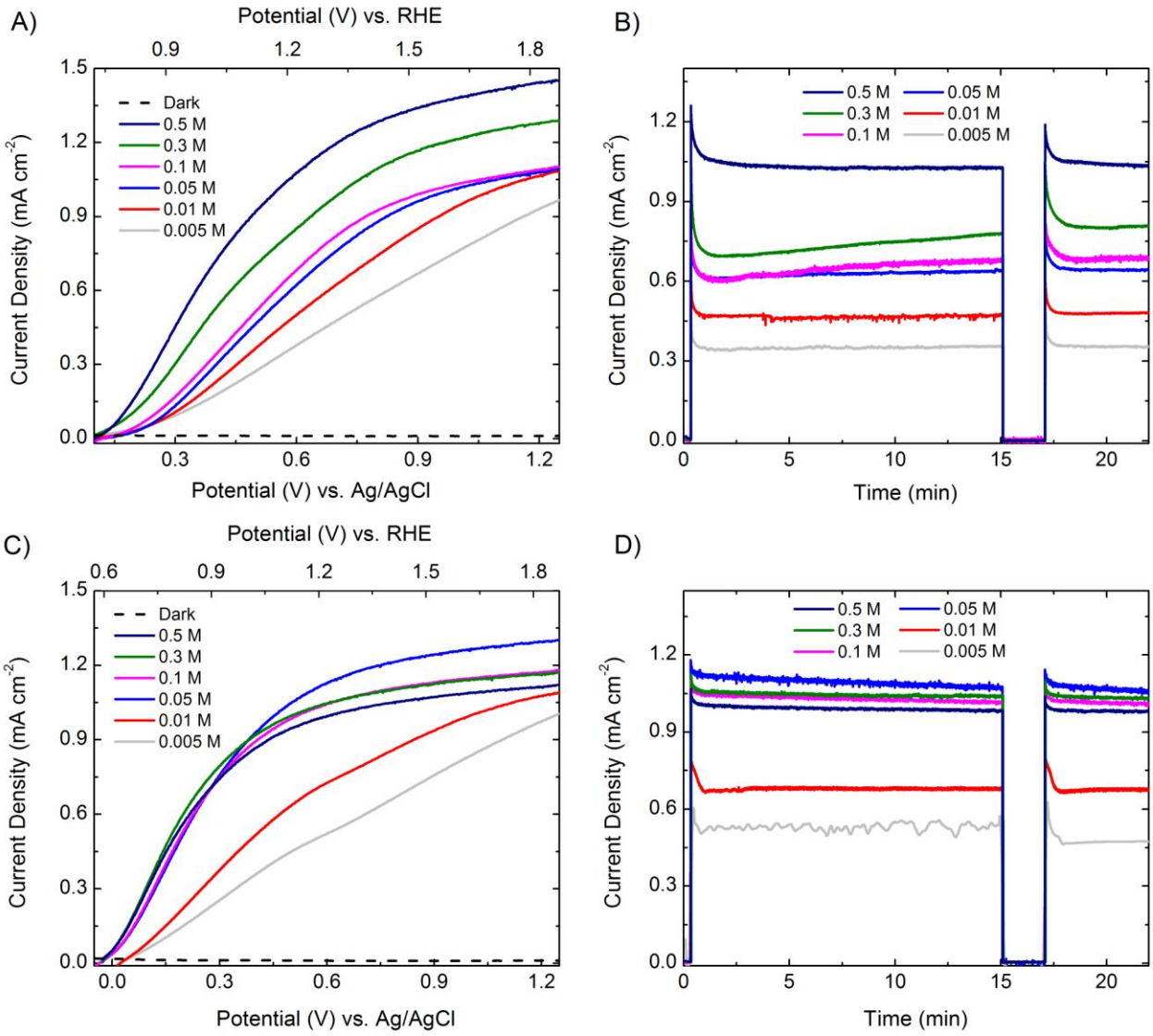

Figure 5. Photoelectrochemical characterization under AM 1.5 G simulated solar light irradiation of the protected WO_3/$BiVO_4$/NiFe photoanodes in contact with (A, B) Na_2SO_4 and (C, D) KPi solutions at pH 7. (A, C) Linear sweep voltammetry, (B, D) chronoamperometry curves recorded at 1.23 V *vs.* RHE.

with different concentration solutions are stable and the value recorded after the initial capacitive spike remains unaltered during the entire test.

The linear sweep voltammetry scans obtained in contact with KPi solutions and reported in Figure 5C indicate that the photocurrent density seems almost unaffected by an increase in KPi concentration above 0.05 M. When in contact with this KPi solution, the $WO_3/BiVO_4$/NiFe electrode generates the highest saturation photocurrent and only a few mV cathodic shift of the photocurrent onset is observed in more concentrated KPi solutions.

As for the stability tests performed in contact with the Na_2SO_4 electrolyte, those performed with the $WO_3/BiVO_4$/NiFe photoanode in KPi solutions at 1.23 V *vs.* RHE (Figure 5D) are in line with the linear sweep voltammetry scans. The photostability in KPi solutions gets extremely improved upon the deposition of the oxygen evolution catalyst. However, also for the NiFe coated electrodes, the KPi solutions are a harsher environment than the Na_2SO_4-containing ones and the photocurrent slightly decreases when the $WO_3/BiVO_4$/NiFe photoanodes are in contact with solutions containing a KPi concentration higher than 0.05 M.

Figure 6A reports a direct comparison between the linear sweep voltammetry curves recorded with the unprotected and with the NiFe protected $WO_3/BiVO_4$ photoanodes in contact with the optimal concentration of Na_2SO_4 and KPi solutions. The deposition of the oxygen evolution catalyst clearly enhances the photoactivity of the $WO_3/BiVO_4$ system by cathodically shifting the photocurrent onset by 310 and 260 mV, in contact with Na_2SO_4 and KPi solutions, respectively. At 1.23 V *vs.* RHE the photocurrent generated by $WO_3/BiVO_4$/NiFe is 2.4 times higher than that generated by the unprotected film in contact with the Na_2SO_4 electrolyte, while in KPi the photocurrent generated by the protected electrode is just 1.3 times higher.

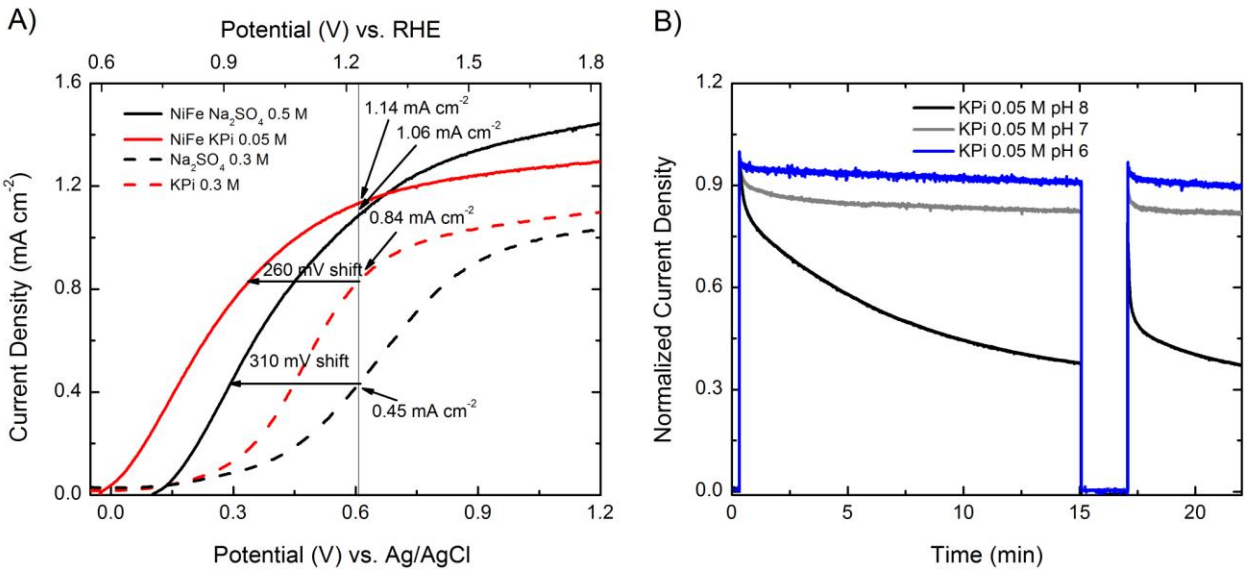

Figure 6. (A) Comparison between the linear sweep voltammetry curves recorded with the unprotected (dashed lines) and NiFe protected (solid lines) $WO_3/BiVO_4$ photoanode in contact with the optimal concentration of KPi and Na_2SO_4 electrolytes (red and black lines, respectively); the vertical line denotes 1.23 V *vs.* RHE, the formal potential of water oxidation. (B) Chronoamperometry traces recorded at 1.23 V *vs.* RHE under AM 1.5 G with the $WO_3/BiVO_4$/NiFe electrode in 0.05 M KPi solution at pH 6, 7 and 8.

The photostability of the $WO_3/BiVO_4$/NiFe electrode in contact with KPi solutions at pH 6 and 8 was also checked, using three freshly prepared $WO_3/BiVO_4$ electrodes (one for each test at different pH), which were individually coated with the NiFe catalyst and activated through 2 h-long irradiation in 0.5 M Na_2SO_4 (this electrolyte does not cause any alteration of the protected photoanodes). The chronoamperometry curves reported in Figure 6B show that the photocurrent quickly drops by 60% of its initial value when the protected photoanode is irradiated in contact with the solution at pH 8. Therefore, though providing stability to the $WO_3/BiVO_4$ photoanode, the NiFe coating failed to efficiently protect the photoanode under such conditions.

CONCLUSIONS

In conclusion, we found that the $WO_3/BiVO_4$ and $WO_3/BiVO_4$/NiFe electrodes produce higher photocurrent when contacted with KPi than with Na_2SO_4 solutions. However, both unprotected and protected electrodes are less stable in contact with KPi solutions. Indeed, the KPi electrolyte seems to promote a photocorrosion process in which photogenerated holes oxidize the photoanode. This hole self-scavenging would account for the higher photocurrent density provided by the photoanodes in contact with KPi with respect to those in contact with Na_2SO_4. On the other hand, both the unprotected and the NiFe-protected electrodes are particularly unstable in contact with basic solutions.

The photocurrent provided by the $WO_3/BiVO_4$ heterojunction system is highly enhanced by deposition of the NiFe co-catayst and the photocurrent onset is cathodically shifted by at least 260 mV. The $WO_3/BiVO_4$/NiFe electrode is more resistant toward photoxidation than the unprotected one, with produced photocurrent remaining substantially unaltered in contact with Na_2SO_4 solutions and slightly decreasing in contact with KPi solutions. We are confident that the results of the present study might help in the choice of the testing conditions of $BiVO_4$-based photoanodes.

ASSOCIATED CONTENT

Supporting Information. Consecutive linear sweep voltammetry curves of a $WO_3/BiVO_4$/NiFe electrode showing its progressive activation; two hour-long chronoamperometry curves of $WO_3/BiVO_4$/NiFe electrode in contact with Na_2SO_4 or KPi electrolytes; emission spectrum of the UV-Vis source; comparison of UV-Vis absorption spectra of $WO_3/BiVO_4$ photoanodes prepared in the same day; Energy Dispersive X-ray spectroscopy (EDX) analysis of $WO_3/BiVO_4$ photoanodes after their photoelectrochemical characterization in different electrolyte solutions; 4 h-long chronoamperometry of $WO_3/BiVO_4$/NiFe electrode performed in 0.5 M Na_2SO_4 aqueous medium. This material is available free of charge via the Internet at http://pubs.acs.org.

AUTHOR INFORMATION

Corresponding Author

* Phone: +39 02 50314237. Fax: +39 02 50314300. E-mail: elena.selli@unimi.it

Notes

The authors declare no competing financial interest.

ACKNOWLEDGMENT

The Regione Lombardia – Fondazione Cariplo joint *SmartMatLab* project (Fondazione Cariplo grant 2013-1766) is gratefully acknowledged. I.G. is thankful to Fondazione Fratelli Confalonieri for a supporting grant.

REFERENCES

(1) Kudo, A.; Ueda, K.; Kato, H.; Mikami, I. Photocatalytic H_2 Evolution under Visible Light Irradiation on $Zn_{1-x}Cu_xS$ Solid Solution. *Catal. Letters* **1998**, *53*, 229–230.

(2) Kudo, A.; Omori, K.; Kato, H. A Novel Aqueous Process for Preparation of Crystal Form-Controlled and Highly Crystalline $BiVO_4$ Powder from Layered Vanadates at Room Temperature and Its Photocatalytic and Photophysical Properties. *J. Am. Chem. Soc.* **1999**, *121*, 11459–11467.

(3) Hong, S. J.; Lee, S.; Jang, J. S.; Lee, J. S. Heterojunction $BiVO_4/WO_3$ Electrodes for Enhanced Photoactivity of Water Oxidation. *Energy Environ. Sci.* **2011**, *4*, 1781–1787.

(4) Moniz, S. J. A.; Zhu, J.; Tang, J. 1D Co-Pi Modified $BiVO_4$ /ZnO Junction Cascade for Efficient Photoelectrochemical Water Cleavage. *Adv. Energy Mater.* **2014**, *4*, 1301590.

(5) Xie, M.; Fu, X.; Jing, L.; Luan, P.; Feng, Y.; Fu, H. Long-Lived, Visible-Light-Excited

Charge Carriers of TiO_2/$BiVO_4$ Nanocomposites and Their Unexpected Photoactivity for Water Splitting. *Adv. Energy Mater.* **2014**, *4*, 1300995.

(6) Pilli, S. K.; Deutsch, T. G.; Furtak, T. E.; Brown, L. D.; Turner, J. A; Herring, A. M. $BiVO_4$/$CuWO_4$ Heterojunction Photoanodes for Efficient Solar Driven Water Oxidation. *Phys. Chem. Chem. Phys.* **2013**, *15*, 3273–3278.

(7) Abdi, F. F.; Savenije, T. J.; May, M. M.; Dam, B.; Van de Krol, R. The Origin of Slow Carrier Transport in $BiVO_4$ Thin Film Photoanodes: A Time-Resolved Microwave Conductivity Study. *J. Phys. Chem. Lett.* **2013**, *4*, 2752–2757.

(8) Park, H. S.; Kweon, K. E.; Ye, H.; Paek, E.; Hwang, G. S.; Bard, A. J. Factors in the Metal Doping of $BiVO_4$ for Improved Photoelectrocatalytic Activity as Studied by Scanning Electrochemical Microscopy and First-Principles Density-Functional Calculation. *J. Phys. Chem. C* **2011**, *115*, 17870–17879.

(9) Berglund, S. P.; Rettie, A. J. E.; Hoang, S.; Mullins, C. B. Incorporation of Mo and W into Nanostructured $BiVO_4$ Films for Efficient Photoelectrochemical Water Oxidation. *Phys. Chem. Chem. Phys.* **2012**, 7065–7075.

(10) Park, Y.; McDonald, K. J.; Choi, K.-S. Progress in Bismuth Vanadate Photoanodes for Use in Solar Water Oxidation. *Chem. Soc. Rev.* **2013**, *42*, 2321–2337.

(11) Meekins, B. H.; Kamat, P. V. Role of Water Oxidation Catalyst IrO_2 in Shuttling Photogenerated Holes Across TiO_2 Interface. *J. Phys. Chem. Lett.* **2011**, *2*, 2304–2310.

(12) Abe, R.; Higashi, M.; Domen, K. Facile Fabrication of an Efficient Oxynitride TaON Photoanode for Overall Water Splitting into H_2 and O_2 under Visible Light Irradiation. *J.*

Am. Chem. Soc. **2010**, *132*, 11828–11829.

(13) Abdi, F. F.; Van de Krol, R. Nature and Light Dependence of Bulk Recombination in Co-Pi-Catalyzed $BiVO_4$ Photoanodes. *J. Phys. Chem. C* **2012**, *116*, 9398–9404.

(14) Zhong, D. K.; Choi, S.; Gamelin, D. R. Near-Complete Suppression of Surface Recombination in Solar Photoelectrolysis by "Co-Pi" Catalyst-Modified W:$BiVO_4$. *J. Am. Chem. Soc.* **2011**, *133*, 18370–18377.

(15) Burke, M. S.; Enman, L. J.; Batchellor, A. S.; Zou, S.; Boettcher, S. W. Oxygen Evolution Reaction Electrocatalysis on Transition Metal Oxides and (Oxy)hydroxides: Activity Trends and Design Principles. *Chem. Mater.* **2015**, *27*, 7549–7558.

(16) Kim, T. W.; Choi, K.-S. Nanoporous $BiVO_4$ Photoanodes with Dual-Layer Oxygen Evolution Catalysts for Solar Water Splitting. *Science* **2014**, *343*, 990–994.

(17) Cai, L.; Zhao, J.; Li, H.; Park, J.; Cho, I. S.; Han, H. S.; Zheng, X. One-Step Hydrothermal Deposition of Ni:FeOOH onto Photoanodes for Enhanced Water Oxidation. *ACS Energy Lett.* **2016**, *1*, 624–632.

(18) Zhang, B.; Zheng, X.; Voznyy, O.; Comin, R.; Xu, J.; Liu, M.; Garcia, de A. F. P.; Dinh, C. T.; Fan, F.; Yuan, M.; et al. Homogeneously Dispersed, Multimetal Oxygen-Evolving Catalysts. *Science* **2016**, *352*, 333.

(19) Seabold, J. A.; Choi, K.-S. Efficient and Stable Photo-Oxidation of Water by a Bismuth Vanadate Photoanode Coupled with an Iron Oxyhydroxide Oxygen Evolution Catalyst. *J. Am. Chem. Soc.* **2012**, *134*, 2186–2192.

(20) Laskowski, F. A. L.; Nellist, M. R.; R, V.; Boettcher, S. Junction Behavior of N-Si

Photoanodes Protected by Thin Ni Elucidated from Dual Working Electrode Photoelectrochemistry. *Energy Environ. Sci.* **2017**, *10*, 570–579.

(21) Mcdowell, M. T.; Lichterman, M. F.; Spurgeon, J. M.; Hu, S.; Sharp, I. D.; Brunschwig, B. S.; Lewis, N. S. Improved Stability of Polycrystalline Bismuth Vanadate Photoanodes by Use of Dual-Layer Thin TiO_2/Ni Coatings. *J. Phys. Chem. C* **2014**, *118*, 19618–19624.

(22) Shi, X.; Jeong, H.; Oh, S. J.; Ma, M.; Zhang, K.; Kwon, J.; Choi, I. T.; Choi, I. Y.; Kim, H. K.; Kim, J. K.; et al. Unassisted Photoelectrochemical Water Splitting Exceeding 7% Solar-to-Hydrogen Conversion Efficiency Using Photon Recycling. *Nat. Commun.* **2016**, *7*, 11943.

(23) Zhang, L.; Reisner, E.; Baumberg, J. J. Al-Doped ZnO Inverse Opal Networks as Efficient Electron Collectors in $BiVO_4$ Photoanodes for Solar Water Oxidation. *Energy Environ. Sci.* **2014**, *7*, 1402–1408.

(24) Yang, P.; Zheng, X. Simultaneously Efficient Light Absorption and Charge Separation in WO_3/$BiVO_4$ Core/Shell Nanowire Photoanode for Photoelectrochemical Water Oxidation. *Nano Lett.* **2014**, *14*, 1099–1105.

(25) Kim, J. H.; Jang, J.-W.; Jo, Y. H.; Abdi, F. F.; Lee, Y. H.; Van de Krol, R.; Lee, J. S. Hetero-Type Dual Photoanodes for Unbiased Solar Water Splitting with Extended Light Harvesting. *Nat. Commun.* **2016**, *7*, 13380.

(26) Abdi, F. F.; Han, L.; Smets, A. H. M.; Zeman, M.; Dam, B.; Van de Krol, R. Efficient Solar Water Splitting by Enhanced Charge Separation in a Bismuth Vanadate-Silicon Tandem Photoelectrode. *Nat. Commun.* **2013**, *4*, 1–7.

(27) Grigioni, I.; Stamplecoskie, K. G.; Jara, D. H.; Dozzi, M. V.; Oriana, A.; Cerullo, G.; Kamat, P. V.; Selli, E. Wavelength-Dependent Ultrafast Charge Carrier Separation in the WO_3 /$BiVO_4$ Coupled System. *ACS Energy Lett.* **2017**, *2*, 1362–1367.

(28) Zhang, H.; Cheng, C. Three-Dimensional FTO/TiO_2 /$BiVO_4$ Composite Inverse Opals Photoanode with Excellent Photoelectrochemical Performance. *ACS Energy Lett.* **2017**, 813–821.

(29) Li, M.; Zhao, L.; Guo, L. Preparation and Photoelectrochemical Study of $BiVO_4$ Thin Films Deposited by Ultrasonic Spray Pyrolysis. *Int. J. Hydrogen Energy* **2010**, *35*, 7127–7133.

(30) Hernández, S.; Thalluri, S. M.; Sacco, A.; Bensaid, S.; Saracco, G.; Russo, N. Photo-Catalytic Activity of $BiVO_4$ Thin-Film Electrodes for Solar-Driven Water Splitting. *Appl. Catal. A Gen.* **2015**, 1–6.

(31) Zhou, M.; Bao, J.; Xu, Y.; Zhang, J.; Xie, J.; Guan, M.; Wang, C.; Wen, L.; Lei, Y.; Xie, Y. Photoelectrodes Based upon Mo:$BiVO_4$ Inverse Opals for Photoelectrochemical Water Splitting. *ACS Nano* **2014**, *8*, 7088–7098.

(32) Park, H. S.; Lee, H. C.; Leonard, K. C.; Liu, G.; Bard, A. J. Unbiased Photoelectrochemical Water Splitting in Z-Scheme Device Using W/Mo-Doped $BiVO_4$ and $Zn_xCd_{1-x}Se$. *ChemPhysChem* **2013**, *14*, 2277–2287.

(33) Kim, J. H.; Magesh, G.; Kang, H. J.; Banu, M.; Kim, J. H.; Lee, J.; Lee, J. S. Carbonate-Coordinated Cobalt Co-Catalyzed $BiVO_4$/WO_3 Composite Photoanode Tailored for CO_2 Reduction to Fuels. *Nano Energy* **2015**, *15*, 153–163.

(34) Kim, J. H.; Jo, Y.; Kim, J. H.; Jang, J. W.; Kang, H. J.; Lee, Y. H.; Kim, D. S.; Jun, Y.; Lee, J. S.; Al, K. I. M. E. T. Wireless Solar Water Splitting Device with Robust Cobalt-Catalyzed, Dual-Doped $BiVO_4$ Photoanode and Perovskite Solar Cell in Tandem: A Dual Absorber Artificial Leaf. *ACS Nano* **2015**, *9*, 11820–11829.

(35) Ding, C.; Shi, J.; Wang, D.; Wang, Z.; Wang, N.; Liu, G.; Xiong, F.; Li, C. Visible Light Driven Overall Water Splitting Using cocatalyst/$BiVO_4$ Photoanode with Minimized Bias. *Phys. Chem. Chem. Phys.* **2013**, *15*, 4589.

(36) Choi, S. K.; Choi, W.; Park, H. Solar Water Oxidation Using Nickel-Borate Coupled BiVO4 Photoelectrodes. *Phys. Chem. Chem. Phys.* **2013**, *15*, 6499.

(37) Coridan, R. H.; Nielander, A. C.; Francis, S. A.; Mcdowell, M. T.; Dix, V.; Chatman, S. M.; Lewis, N. S. Methods for Comparing the Performance of Energy-Conversion Systems for Use in Solar Fuels and Solar Electricity Generation. *Energy Environ. Sci.* **2015**, *8*, 2886–2901.

(38) Grigioni, I.; Stamplecoskie, K. G.; Selli, E.; Kamat, P. V. Dynamics of Photogenerated Charge Carriers in WO_3/$BiVO_4$ Heterojunction Photoanodes. *J. Phys. Chem. C* **2015**, *119*, 20792–20800.

(39) Su, J.; Guo, L.; Yoriya, S.; Grimes, C. A. Aqueous Growth of Pyramidal-Shaped $BiVO_4$ Nanowire Arrays and Structural Characterization: Application to Photoelectrochemical Water Splitting. *Cryst. Growth Des.* **2010**, *10*, 856–861.

(40) Kohl, P. A.; Bard, A. J. Semiconductor Electrodes: V . The Application of Chemically Vapor Deposited Iron Oxide Films to Photosensitized Electrolysis. *J. Electrochem. Soc.* **1976**, *123*, 1024–1026.

(41) Su, J.; Feng, X.; Sloppy, J. D.; Guo, L.; Grimes, C. A. Vertically Aligned WO_3 Nanowire Arrays Grown Directly on Transparent Conducting Oxide Coated Glass: Synthesis and Photoelectrochemical Properties. *Nano Lett.* **2011**, *11*, 203–208.

(42) Su, J.; Guo, L.; Bao, N.; Grimes, C. A. Nanostructured $WO_3/BiVO_4$ Heterojunction Films for Efficient Photoelectrochemical Water Splitting. *Nano Lett.* **2011**, *11*, 1928–1933.

(43) Pihosh, Y.; Turkevych, I.; Mawatari, K.; Asai, T.; Hisatomi, T.; Uemura, J.; Tosa, M.; Shimamura, K.; Kubota, J.; Domen, K.; et al. Nanostructured $WO_3/BiVO_4$ Photoanodes for Efficient Photoelectrochemical Water Splitting. *Small* **2014**, *10*, 3692–3699.

(44) Toma, F. M.; Cooper, J. K.; Kunzelmann, V.; McDowell, M. T.; Yu, J.; Larson, D. M.; Borys, N. J.; Abelyan, C.; Beeman, J. W.; Yu, K. M.; et al. Mechanistic Insights into Chemical and Photochemical Transformations of Bismuth Vanadate Photoanodes. *Nat. Commun.* **2016**, *7*, 1–11.

(45) Favaro, M.; Abdi, F. F.; Lamers, M.; Crumlin, E. J.; Liu, Z.; Van de Krol, R.; Starr, D. E. Light-Induced Surface Reactions at the Bismuth Vanadate/Potassium Phosphate Interface. *J. Phys. Chem. B* **2018**, *122*, 801–809.

(46) Sci, C.; Le Formal, F.; T, N.; Cornuz, M.; Moehl, T.; Gr, M.; Sivula, K. Passivating Surface States on Water Splitting Hematite Photoanodes with Alumina Overlayers. *Chem. Sci.* **2011**, *2*, 737–743.

(47) Bornoz, P.; Abdi, F. F.; Tilley, S. D.; Dam, B.; Van de Krol, R.; Grätzel, M.; Sivula, K. A Bismuth Vanadate-Cuprous Oxide Tandem Cell for Overall Solar Water Splitting. *J. Phys. Chem. C* **2014**, *118*, 16959–16966.

(48) Butler, M. A. Prediction of Flatband Potentials at Semiconductor-Electrolyte Interfaces from Atomic Electronegativities. *J. Electrochem. Soc.* **1978**, *125*, 228.

(49) Xu, Y.; Schoonen, M. A. A. The Absolute Energy Positions of Conduction and Valence Bands of Selected Semiconducting Minerals. *Am. Mineral.* **2000**, *85*, 543–556.

(50) Santato, C.; Ulmann, M.; Augustyński, J. Photoelectrochemical Properties of Nanostructured Tungsten Trioxide Films. *J. Phys. Chem. B* **2001**, *105*, 936–940.

(51) Sun, K.; McDowell, M. T.; Nielander, A. C.; Hu, S.; Shaner, M. R.; Yang, F.; Brunschwig, B. S.; Lewis, N. S. Stable Solar-Driven Water Oxidation to O_2(g) by Ni-Oxide-Coated Silicon Photoanodes. *J. Phys. Chem. Lett.* **2015**, *6*, 592–598.